Computer simulation of gene detection without PCR by single molecule detection

Lloyd M. Davis,[a] John G.K. Williams,[bc] and Don T. Lamb[b]

[a]Center for Laser Applications, University of Tennessee Space Institute, Tullahoma, Tennessee 37388, USA

[b]Pioneer Hi-Bred International, P.O. Box 256, Johnston, Iowa 50131, USA

[c]Present Address: LI-COR, Inc., P.O. Box 4000, Lincoln, Nebraska 68504-5000, USA

ABSTRACT

Pioneer Hi-Bred is developing a low-cost method for rapid screening of DNA, for use in research on elite crop seed genetics. Unamplified genomic DNA with the requisite base sequence is simultaneously labeled by two different colored fluorescent probes, which hybridize near the selected gene. Dual-channel single molecule detection (SMD) within a flow cell then provides a sensitive and specific assay for the gene. The technique has been demonstrated using frequency-doubled Nd:YAG laser excitation of two visible-wavelength dyes. A prototype instrument employing infrared fluorophores and laser diodes for excitation has been developed. Here, we report results from a Monte Carlo simulation of the new instrument, in which experimentally determined photophysical parameters for candidate infrared dyes are used for parametric studies of experimental operating conditions. Our findings demonstrate the feasibility of the approach for selected fluorophores, and identify suitable operating conditions. Fluorophore photostability is found to be a key factor in determining the instrument sensitivity. Most infrared dyes have poor photostability, resulting in inefficient SMD. However, the normalized cross-correlation function of the photon signals from each of the two channels can still yield a discernable peak, provided that the concentration of dual-labeled molecules is sufficiently high. Further, for low concentrations, processing of the two photon streams with Gaussian weighted sliding sum digital filters and selection of simultaneously occuring peaks can also provide a sensitive indicator of the presence of dual-labeled molecules, although accidental coincidences must be considered in the interpretation of results.

Keywords: single molecule detection, Monte Carlo simulation, gene detection, DNA hybridization, ultrasensitive, fluorescence, infrared dyes

1. INTRODUCTION

There exists a need for a low-cost high-throughput automatable method for the detection and quantification of small amounts of DNAs that have specific base sequences or contain specific genes. Methods currently in use for such analyses usually require amplification of the DNA by polymerase chain reaction (PCR), which may introduce uncertainties due to contamination and other causes, and they generally involve manually intensive procedures, such as casting gels. Emerging technologies, such as gene chips and microarrays, which achieve massive parallelization by use of a large number of different hybridization probes attached to a surface in a pixelled array, offer the prospect for considerably faster and cheaper DNA analyses. However, in many applications, it is only necessary to perform an assay for one or two known genes, and such technology may not be the most cost-effective means for automation.

In its ongoing research to develop new seeds with desirable genetic traits, Pioneer Hi-Bred annually performs over 0.5 million genotype analyses, and it could well use a much higher number if not for the time and cost. Recently, workers at Los Alamos National Laboratory and Pioneer developed a new highly-sensitive technique for the detection of specific genes in unamplified DNA.[1] As a demonstration of the technique, DNA from a transformed maize plant containing a single copy of a BT (*B. thuringiensis* toxin) transgene was shown to be distinguishable from DNA obtained from plants without the transgene within a measurement time of 10–100 s. The new technique uses dual-channel single-molecule detection (SMD) within a flow cell to perform a sensitive and highly-specific assay for DNAs that are simultaneously labeled by two different hybridization probes, each covalently linked to a differently-colored

L.M.D.: E-mail: ldavis@utsi.edu J.G.K.W.: E-mail: johnw@bio.licor.com D.T.L.: E-mail: lambdt@phibred.com

Part of the EUROPTO Conference on Biomedical Optical Systems and Laser-Assisted Biotechnology
Stockholm, Sweden • September 1998
SPIE Vol. 3570 • 0277-786X/99/$10.00

fluorophore. The two hybridization probes have 15-base sequences such that they bind near to each other at the sought gene. The presence of the sought gene is hence indicated by detection of both colored-fluorophores simultaneously. Free hybridization probes, and DNAs that by chance are labeled by one or the other of the hybridization probes, can generate simultaneous SMD signals only on the rare occasions that two such molecules happen to pass simultaneously. Other analyses, such as determination of the size of specific target DNAs by single molecule electrophoresis, could in principle also be incorporated.[1]

In the Los Alamos experiments, a frequency-doubled mode-locked Nd:YAG laser was used for excitation of two visible wavelength fluorophores, rhodamine 6G and bodipy TR. These dyes have excellent photostability and fluorescence quantum efficiency. They both absorb well at the 532 nm laser wavelength, but have non-overlapping emission spectra, thereby enabling collected light to be separated by a dichroic mirror into two detection channels. The laser was mode-locked at 82 MHz and time-gated photon detection was used to discriminate against Raman scattered light, which originates from the solvent.

Pioneer subsequently embarked on the development of an instrument employing more cost-effective and compact laser diodes for sample excitation. Infrared excitation affords considerably lower background from sample contaminants and induced fluorescence. However, infrared fluorophores generally have low fluorescence quantum efficiency Φ_f and high photodestruction efficiency Φ_D in aqueous solutions. The choice of suitable fluorophores is therefore considerably more limited. In this paper, we consider the following three dyes: NN 382 and IRD 700, available from LI-COR Inc., (http://www.licor.com/) and La Jolla Blue (LJB), available from DIATRON (http://www.diatronscience.com/). Approximate measurements were made of the photodestruction efficiencies of these dyes using the SMD apparatus and a previously reported technique.[2] The photodestruction efficiency results, and the values for the other photophysical parameters required for the simulations, as obtained from the suppliers, are listed in Table 1.

Table 1. Photophysical parameters of fluorophores in aqueous solution.

Fluorophore	NN 382	IRD 700	LJB
fluorescence quantum efficiency Φ_f	0.34	0.5	0.7
molar absorptivity @ 685 nm ($M^{-1}cm^{-1}$)	28,452	170,000	185,771
molar absorptivity @ 780 nm ($M^{-1}cm^{-1}$)	160,198	0	0
photodestruction efficiency Φ_D	1.5×10^{-5}	1.3×10^{-2}	1.8×10^{-5}

Two laser diode excitation wavelengths are required to set up the dual-channel detection scheme with these dyes. The dye NN 382 has its absorption maximum at 780 nm, whereas IRD 700 and LJB absorb strongly at 685 nm. Two 80 MHz sub-nanosecond pulsed laser diodes (Picoquant) were therefore used for sample excitation and time-gated detection at these wavelengths. The power available from each laser diode was limited to below 1 mW, a factor of about 5 lower than that of the frequency-doubled Nd:YAG laser beam used in the Los Alamos experiments. In preliminary experiments using NN 382 and IRD 700, detection of photon bursts could be achieved for each of the dyes, but simultaneous detection of bursts from a sample of DNA labeled by both dyes, or from a sample of covalently-linked dyes, could not be achieved. In order to help determine why simultaneous detection was not achieved, and to determine if it should be more readily achievable if experimental conditions were to be altered, a Monte Carlo simulation of the dual-channel instrument, which is illustrated in Fig. 1, was developed. The model and code for the simulation were adapted from that for a single-channel experimental set-up, which has been reported in detail in Ref. 3.

2. MONTE CARLO SIMULATION

2.1. Major modifications

The major modifications to the previously reported simulation[3] included making appropriate approximations to allow simplification of the code so that it would run faster, and extending the code to consider (1) different types of molecules labeled by arbitrary numbers of different fluorophores with specified photophysical parameters, (2) two or more laser excitation beams of different wavelengths and focal conditions, (3) signal collection by two opposing microscope

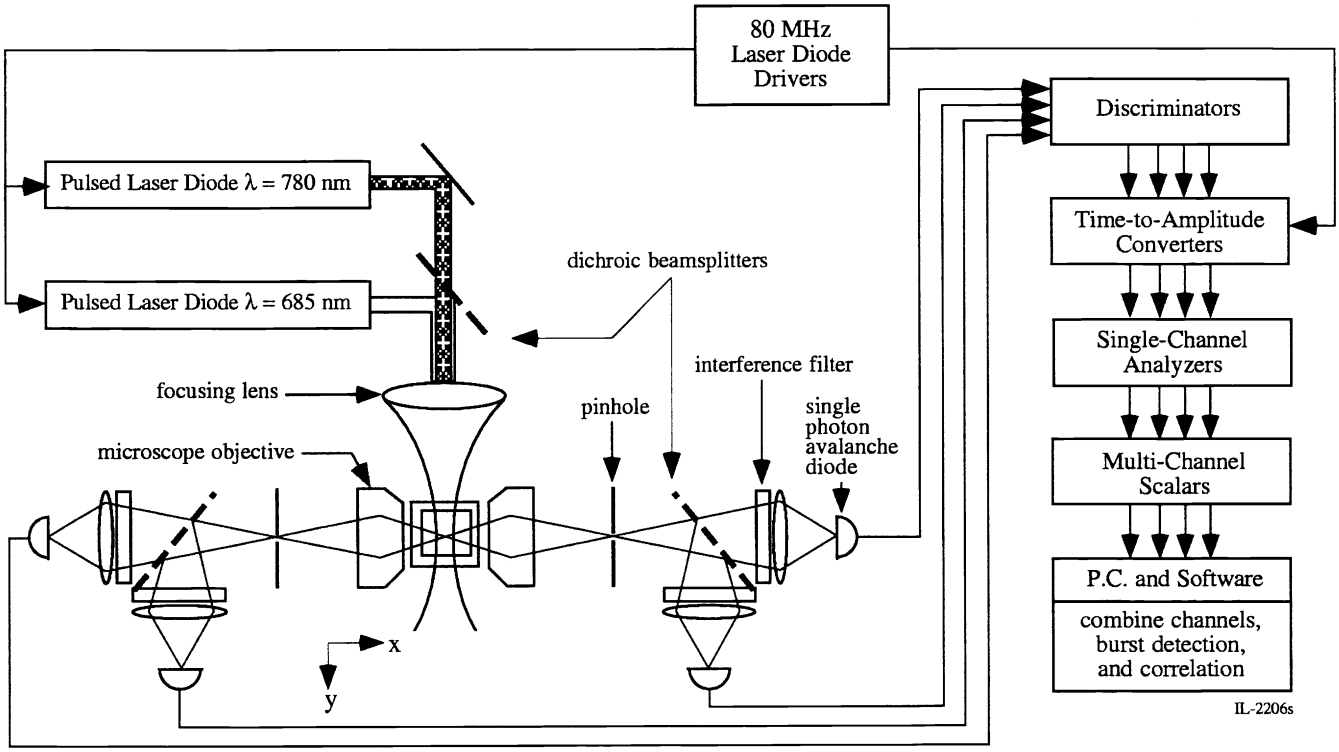

Figure 1. Experimental set-up to be modeled.

objectives, and separation of the collected fluorescence by dichroic filters onto four single photon avalanche diodes (SPADs), (4) addition of the SPAD photon signals, and real-time accumulation of the cross-correlation functions between each of the resulting data acquisition channels. Also, signal processing to watch for simultaneously occuring photon bursts in each of the channels has recently been added to the code.

The extension of the code was such that the program could be used to investigate a wide range of experimental configurations and situations beyond that of Fig. 1, as required for the initial task, including simulations of more complex experiments involving multiple detection zones and electrophoretic separation of different molecular species for DNA sizing. However, this paper reports results only for the two-color one-detection-zone set-up, with no additional electrophoretic separation of molecules. The simulation begins by reading a file of data, which establish the geometry and conditions to be simulated. Table 2 gives the structure of this data file and thereby also indicates the scope of the simulation possibilities. The values of the parameters listed in Table 2 are those used to obtain the first of the results described in section 3 below.

2.2. Approximations and outline of simulation algorithm

With each iteration, the simulation considers (i) the delivery of new molecules into the simulation volume, (ii) the transport of molecules by the solution flow, electrophoresis, and Einstein-Stokes diffusion, (iii) the excitation and subsequent photodegradation of each fluorophore present, (iv) the excitation of fluorophores and subsequent collection and detection of a photon, and (v) removal of molecules due to transport out of the simulation volume, or photodegradation of the last fluorophore attached to a molecule. Also, whenever a photon is detected, the simulation updates the data processing. The major approximations made in simulating the above processes were as follows:

(1) The transport of molecules by the solution flow is assumed to be laminar and uniform. This approximation is justified because the actual velocity profile within a square cross-section capillary is approximately parabolic and cylindrically symmetric about the center of the square, and the decrease in velocity with distance from the center

Table 2. Simulation input file structure, giving parameters for results of Figure 2–4. Parameters indicated by * may be interactively altered during program execution.

Parameter description	Value	Parameter description	Value
simulation time duration (s)	100.0	no. of collection lenses and pinholes	2
time step/electronic dead-time (s)	1.0e-6	x, y-location of object space (μm)	0.0, 0.0
volumetric flow rate (μl/min)	50.0*	z-location of object space (μm)	10.0
square capillary size ID (μm)	500.0	spatial filter pinhole radius (μm)	300
total dye concentration (M)	1.0e-13*	magnification	40
molecules are introduced from a		numerical aperture	0.85
square column of this size @$z = 0$	20.0	[add 6 lines per lens/pinhole]	
molecules are removed at this z	20.0	next 6 parameters:	
number of laser wavelengths (#w)	2	0.0, 0.0, 10.0, 300, 40, 0.85	(lens 2)
wavelength of 1st laser (μm) λ_1	0.685	number of SPAD detectors	4
[add 1 line per wavelength]		no. of lens/pinhole used by 1st SPAD	1
next 1 parameter: 0.780	(λ_2)	data analysis channel to which	
number of fluorophore types (#f)	2	photocounts are summed	1
fluor. absorptivity (/M/cm) @λ_1	170000	dark counts (/s) in time window	100
fluor. absorptivity (/M/cm) @ λ_2	0	counts (/s) with 1st laser beam on	1100
[add 1 line per wavelength]		counts (/s) with 2nd laser beam on	100
fluor. quantum efficiency Φ_f	0.5	[add 1 line per laser beam]	
photodestruction efficiency Φ_D	1.3e-2	filter & time-gate throughput for 1st fluor.	0.6, 0.4
[add 2+#w lines per fluorophore]		filter & time-gate throughput for 2nd fluor.	0.0, 0.4
next 4 parameters:		[add 2 parameters per fluorophore type]	
28452, 160198, 0.34, 1.5e-5	(fluor. 2)	other optics throughput	0.9
number of molecule types (#m)	3	quantum efficiency of SPAD	0.65
fraction of 1st molecule type	0.98	[add 5+2#f+#b lines per SPAD]	
no. of fluorophores of 1st type	1	next 35 parameters:	
no. of fluorophores of 2nd type	1	1, 2, 100, 100, 2100, 0.6, 0.4, 0.0, 0.4, 0.9, 0.65	(SPAD 2)
[add 1 line per fluorophore type]		1, 1, 100, 1100, 100, 0.0, 0.4, 0.6, 0.4, 0.9, 0.65	(SPAD 3)
diffusion coefficient (μm^2/s)	4.5e1	1, 2, 100, 100, 2100, 0.6, 0.4, 0.0, 0.4, 0.9, 0.65	(SPAD 4)
electrophoretic velocity (μm/s)	0.0e4	number of data analysis channels	2
[add 3+#f lines per molecule type]		std. dev. of Gaussian weights (s)	$5.07 \times 10^{-4\dagger}$
next 10 parameters:		† half-transit time δ_t through beam 1	
0.01, 1, 0, 4.5e2, 0.0e4,	(mol. 2)	threshold for peak detection	8.5*
0.01, 0, 1, 4.5e2, 0.0e4	(mol. 3)	[add 2 lines per analysis channel]	
number of laser beams (#b)	2	next 2 parameters: 5.22×10^{-4}, 11.5*	(ch. 2)
wavelength no. of 1st beam	1	display graph of photon bursts	1
y, z-locations of beam waist (μm)	0.0, 8.0	y, t-scale for graph (photons, s)	100, 0.2
waist size (μm)	3.5	indicate individual photons on graph	1
power (W)	5.0e-4*	display graph of molecule trajectories	1
[add 5 lines per beam]		display from where photons originate	0
next 5 parameters:		calculate & graph normalized correlations	1
2, 0.0, 8.0, 3.6, 1.0e-3*	(beam 2)	y, t-scale for graph (dimensionless, s)	2.5, 0.001

will be negligible for distances small compared to the cell dimensions. For a perfect square cross-section of inside dimensions $l \times l$, the velocity at the center is $2.09 \times \bar{v}$, where the mean velocity is $\bar{v} = V/l^2$, and V is the volumetric flow rate.[4] Hence, for a 500μm square capillary with slightly rounded corners, if V is expressed in μl/min, we take $v \approx 1.38 \times 10^2 \times V$, where v is in μm/s. The mean half-transit-time across a laser beam of waist radius ω_0 is then $\delta t = \omega_0/v$.

(2) The irradiance profile of each laser beam was assumed to be independent of the beam propagation direction, x. Thus, if a molecule is located at x, y, z, the irradiances it is subject to are given by

$$I_\lambda = (2P/\pi\omega_0^2) \exp[-2(y^2 + z^2)/\omega_0^2], \tag{1}$$

where P is the laser power, and ω_0 is the measured beam waist. The neglect of the change in the beam radius with x is valid provided that the Rayleigh range $x_0 = \pi\omega_0^2 n/\lambda$ multiplied by the collection lens magnification is greater than the pinhole radius, which for the parameters of Table 2 yields 75μm $\times 40 \gg 300\mu$m. Here, n is the refractive index of the solution, 1.33.

(3) Saturation effects were neglected in considering the fluorophore excitation. Thus for a fluorophore f with absorption cross-section $\sigma_f(\lambda)$ at the laser excitation wavelength λ, the mean rate of excitation per second when subject to laser irradiances I_λ is

$$K_f = \sum_\lambda I_\lambda \, \zeta \, \sigma_f(\lambda)/E_\gamma(\lambda), \tag{2}$$

where $\zeta = \cos^2\theta$ is a dimensionless parameter to account for the angle θ between the fluorophore transition dipole moment and the laser excitation polarization direction, and $E_\gamma(\lambda) = hc/\lambda$ is the photon energy. The absorption cross-section $\sigma_f(\lambda)$ in units of μm^2 is $5.7 \times 10^{-13} \times$ the molar absoptivity, in units of $\mathrm{M^{-1}cm^{-1}}$. The probability for excitation per laser pulse is K_f/R, where R is the 8×10^7 s^{-1} excitation laser repetition rate. The neglect of saturation effects is valid provided $K_f/R \ll 1$. (Also, as discussed in Ref. 3, the duration of the laser pulses must be longer than the 1 ps time required for thermalization of the fluorophore excited-state vibrational manifold, if the effects of stimulated emission on the net excitation rate are to be neglected.) For the parameters of Table 2, $K_f/R \ll 1$ even for a molecule at the center of the Gaussian beam waist and with $\zeta = 1$, provided that the laser power is $P \ll 4.3$ mW. This is certainly the case for the sub-milliwatt laser diode powers under consideration.

(4) The fluorophore phosphorescence lifetime, which results in a molecular 'dead-time' effect whenever intersystem crossing of a fluorophore to the triplet manifold occurs, was assumed to be comparable to, or shorter than the dead time of the electronics. The phosphorescence lifetimes of the fluorophores under investigation are not known, but for most fluorophores values of $\sim 10^{-6}$s are typical. By comparison, the time-to-amplitude converters used for time-gated single photon counting have dead-times of $\sim 1 \times 10^{-6}$s (determined by the pulse-widths of the output pulses). Dead-time effects, whether due to molecular dead-time or electronic dead-time, are accounted for in the simulation by selecting the iteration time-step Δt to be equal to the 1 μs dead-time. Within each iteration time-step there are 80 laser excitation pulses, but at most only one photon can be detected during this time from each SPAD.

Intersystem crossing reduces the net fluorescence quantum efficiency in the same manner as any other process that competes with fluorescence does. It is assumed that the steady state measured values of the fluorescence quantum efficiencies of the fluorophores listed in Table 1 already account for intersystem crossing as a quenching mechanism. Thus, when a fluorophore f is present, the probability for detection of a fluorescence photon per time-step is taken to be

$$P_f = K_f \, \Delta t \, \Phi_f \, C(x,y,z) \, F_f \, E_f, \tag{3}$$

where Φ_f is the net fluorophore quantum efficiency, $C(x,y,z)$ is the geometric collection efficiency, F_f is the throughput of the interference filter and remaining optics $\times$ the SPAD quantum efficiency for the emmision of fluorophore f, and E_f is the throughput of the time-gate for the decay profile of fluorophore f.

(5) The rotational diffusion lifetimes of the fluorophore-labeled DNAs are considerably shorter than the time-step Δt so that the geometric average of the orientation factor $\bar{\zeta} = \iint \zeta \cos\theta \, d\theta d\phi = 1/3$ is used when evaluating the mean excitation rate K_f.

With each iteration, a random number with uniform distribution between 0 and 1 is generated. If the number is between 0 and P_b, a background photon is assumed to have been detected, where P_b is the experimentally determined background photon rate $\times \Delta t$. If the number is between P_b and $P_b + P_f$, a fluorescence photon is assumed to have

been detected. Dead-time effects, either due to fluorophore intersystem crossing, or the electronics, will be negligible provided $P_b/E_b + P_f/E_f \ll 1$. For the parameters given in Table 2, for a single fluorophore of NN 382 at the origin with $\bar{\zeta} = 1/3$, $K_f/R = 0.077$, the maximum net collection efficiency for each SPAD is $C(0,0,0)\,F_f = 4.04 \times 10^{-2}$, and $P_f/E_f \approx 0.125$. Also, the typical time-gate efficiency for background counts is $E_b = 0.1$, so that $P_b/E_b = 20100$ $s^{-1} \times 1 \times 10^{-6}s = 0.02$. These numbers indicate that dead-time effects are expected to be small, unless there are a large number of fluorophores simultaneously present at the center of the probe region.

(6) In evaluating $C(x,y,z)$, the net collection efficiency of fluorescence from a fluorophore located at x,y,z, a geometric optics or ray-tracing formula is used. The maximum geometric collection efficiency $\hat{C}$, which is obtained for a fluorophore at the origin, is determined by the numerical aperture of the collection lens, NA, and is given by

$$\hat{C} = [1 - \cos(\sin^{-1}(\mathrm{NA}/n))]/2. \tag{4}$$

If the fluorophore is not at the origin, the collection lens will image the fluorescence to a defocused and decentered circular disk. The overlap between this disk and the circular spatial-filter pinhole determines the reduction in the geometric collection efficiency relative to this maximum value, and is given in equation (28) of Ref. 3. Note that there is a double-conic shaped region about the origin, throughout which the defocused, decentered image still passes completely through the spatial-filter pinhole. The overlap of this region of full collection efficiency with the laser beam defines the probe region.

(7) In the simulation, the position x,y,z of each molecule, the irradiance $I(y,z)$ it is subject to, the collection efficiency from the molecule $C(x,y,z)$, and other derived quantities, are not updated with each iteration, but only when the molecule is expected to have moved a distance of $\sim \omega_0/20$. The mean distance that a molecule moves during a time ΔT is $v\Delta T$ due to the linear flow and $\sqrt{2D\Delta T}$ due to diffusion, where D is the diffusion coefficient. For the parameters of Table 2, $v\Delta t \gg \sqrt{2D\Delta t}$, and hence the update occurs each m iterations, where $m \approx \omega_0/20v\Delta t \approx 25$.

2.3. Data processing and cross-correlation algorithm

As outlined above, with each iteration, each SPAD detector and time-gate circuit may yield either 0 or 1 photons. If a photon is generated, it is known whether the photon originated from background, or a particular type of fluorophore. Such information cannot be known in the experiment, but it is known and used in the simulation to develop statistics on the success of SMD. The simulation uses the streams of detected photons to generate the weighted-sliding-sum curves. Photon bursts yield a peak in the weighted-sliding-sum curve. If the peak is above a preset threshold, the simulation will record the peak as a detection event. In any case, the program looks back at each of the photons that comprise each burst, that is those photons that fall within $\pm 1.5 \times \delta t$ with respect to the peak of the burst. If all of these photons originated from background, then the peak is catagorized as a background event. If at least one of the photons originated from a fluorophore of type f, then the peak is catagorized as being caused by that fluorophore. If photon bursts occur in both data analysis channels within a time equal to the larger of the two values of $1.5 \times \delta t$, the bursts are deemed to be simultaneous. The simulation sorts simultaneous photon bursts that are due to either fluorophore type from simultaneous bursts in which one or both peaks were caused by background.

The simulation also accumulates the autocorrelation function of the photon stream recorded in each detection channel and the cross-correlation functions between each of the channels. The algorithms used for calculation of the weighted-sliding-sum and the correlation functions are particularly fast and hence are detailed below:

For each data analysis channel, the delay or number of iterations separating each detected photon are recorded in an array, defined by the C code:

```
long unsigned int delay[number_of_channels][1000];
```

Only the last 1000 such delays are retained and the array is then overwritten. To accomplish this, with every iteration, the number of iterations since the last photon detection is incremented for each of the channels:

```
for(c=0; c<number_of_channels; c++) delay[c][photon_number[c]] ++;
```

When a photon is detected by either of the two SPADs assigned to channel `c`, the index into the array of delays, `photon_number[c]`, is advanced using the following C statements:

```
photon_number[c] = (photon_number[c]==999 ) ? 0 : photon_number[c]+1;
delay[c][photon_number[c]] = 0;
```

(Note that if two or more photons are detected in one channel within the same iteration, the recorded delay between such photons will be 0.)

The array of delays is used to evaluate the weighted sliding sum for each of the analysis channels using equation (40) in Ref. 3. The weights, which are taken to be a Gaussian function corresponding to the expected signal versus time for a fluorophore that passes through the laser beam without diffusion or photodegradation, are stored in an array prior to the simulation. This array is defined by:

```
float w[c][w_limit[c]];
for(c=0; c<number_of_channels; c++)
    for(j=0; j<w_limit; j++) w[c][j] =  sqrt(2) * exp( -((j-dt[c])/dt[c])**2 );
```

where `dt[c]`$= \delta t$, the mean half-transit-time for each of the data analysis channels, and `w_limit[c] = 2*dt[c]+1`.

The C code for evaluating the weighted sliding sum, which is executed only when a photon is detected but before advancing `photon_number[c]`, is as follows:

```
remainder[c] += delay[photon_number[c]];
while(remainder[c]>dt[c]/4) {
    remainder[c]-=dt[c]/4;
    y = 0.0;  x++;
    p=photon_number[c];
    for( i=delay[c][p]-remainder[c]; i<w_limit[c]; p=(p==0) ? 999 : p-1, i+=delay[c][p])
        y+= w[c][i];
    }
```

The algorithm used for accumulation of all correlation functions is an extension of the algorithm described in Ref. 3 for acquisition of the autocorrelation function in a single channel set-up. It basically works by counting the number of time-steps between all possible photon pairs that occur in each analysis channel to determine the delay τ, and then incrementing the correlation function at each such τ. The code for this process, which is executed after advancing `photon_number[c]` when a photon is detected in channel `c`, is as follows:

```
for( c1=0; c1<number_of_channels; c1++) {
    p=photon_number[c];
    for(sum_delay=delay[c][p]; sum_delay<G_limit; p=(p==0)?999:p-1, sum_delay+=delay[c1][p])
        G[c][c1][sum_delay] ++;
    }
```

Here, the cross-correlation functions are accumulated within the array defined by

```
long unsigned int G[number_of_channels][number_of_channels][G_limit]={0};
```

The interpretation of the array in terms of the digital correlation functions is as follows: If the signal in each of a number of channels is $s_n(t)$, then

$$G[i][j](\tau) = \sum_t s_i(t)\, s_j(t+\tau), \tag{5}$$

where the delay $\tau \geq 0$. For two analysis channels, the complete cross-correlation function for both positive and negative delays is hence obtained by combination of $G[0][1](\tau)$ and $G[1][0](\tau)$. Note that ideally $G[0][1](0) = G[1][0](0)$. Note also that

$$G[i][i](0) = \sum_t [s_i(t)]^2. \tag{6}$$

The values from equation 6 are used to determine the normalized correlation functions[5] as follows:

```
for(j=0; j<G_limit; j++)
g[c][c1][j] = G[c][c1][j] * number_of_iterations / (G[0][0][0] * G[1][1][0] );
```

where `number_of_iterations` is the total number of simulation iterations over which the arrays were accumulated.

The normalized correlation functions will assymptotically approach unity for long delays. They have peak values that are independent of the data acquisition time, but indicative of the net departure from random Poissonian photon statistics due to the photon bursts within a channel, or the correlated photon signals between channels. There is no theoretical limit to the magnitude of the peak. The normalized cross-correlation functions are sensitive to correlated photons embedded in data consisting of a large Poissonian background, or a large number of uncorrelated photon bursts. However, if the total fluorophore concentration is sufficiently low to avoid accidental coincidences, the watch for simultaneously occuring peaks in the weighted sliding sum from each channel can provide an even more sensitive indicator.

3. RESULTS AND DISCUSSION

The simulation indicates that SMD is easily achievable for NN 382 but only barely achievable for IRD 700. Almost all IRD 700 fluorophores become photodestroyed as they approach the edge of the detection volume, resulting in small photon burst amplitudes, which are seldom above the level of the background fluctuatiuons. Figure 2 displays the histogram of burst amplitudes from each channel under the conditions of Table 2. The threshold is set at the lowest level for which the number of detection events exceeds the number of background fluctuation events, that is 8.5 for channel 0, which is sensitive to the 0.5 mW 685 nm beam, and 11.5 for channel 1, which is sensitive to the 1 mW 780 nm beam. The volumetric flow rate is such that the flow velocity is $v = 6.9\mu$m/ms and the mean half-transit time for IRD 700 fluorophores across a 3.5 μm beam waist radius is $\delta t = 0.507$ ms. For the probe volume cross-sectional area of 7 μm$\times$15μm and the IRD 700 concentration of 0.99×10^{-13} M, 4316 molecules are expected to pass through the probe region during the 100 s simulation time. However, there are only 184 peaks due to molecules (and 54 peaks due to background) above the threshold, corresponding to a detection efficiency of $< 5\%$. The mean number of molecules that pass through the detection volume during the $2\delta t$ time imposed by the weighted sliding sum filter is $\mu = 43.16\ \mathrm{s}^{-1} \times 2\delta t = 0.04376$ and hence the fraction of molecules expected from Poissonian statistics to pass individually is $\mu e^{-\mu} - 1 = 0.978$. Thus as many as 95 $[(1 - 0.978) \times 4316]$ of the 184 detected peaks could be due to two or more molecules passing simultaneously through the detection volume. The photostability for NN 382 is almost 100 times better than that of IRD 700. This allows larger photon bursts to be obtained by use of higher laser excitation power. In Fig. 2b, there are 3882 peaks due to molecules (and 148 peaks due to background) above a threshold of 11.5, corresponding to a detection efficiency of ~ 90 %.

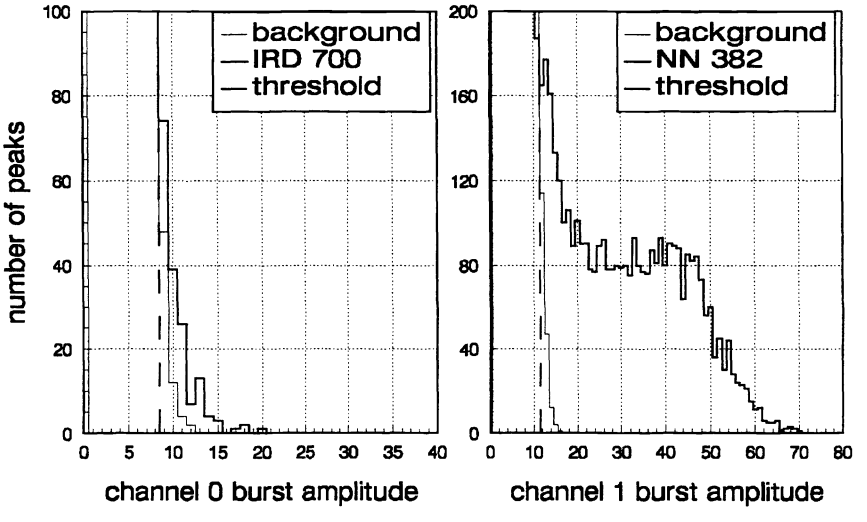

Figure 2. Histograms of Gaussian weighted sliding sum peak amplitudes, due to background fluctuations and passage of (a) IRD 700 fluorophores, and (b) NN 382 fluorophores.

Peaks from channel 0 that occur simultaneously within $\pm 1.5 \times 0.507$ ms of a peak from channel 1 are sorted in the data analysis. Figure 3 shows a plot of the amplitudes in channels 0 and 1 of such simultaneous peaks. Above threshold settings of 8.5 and 11.5, there are 75 simultaneously occurring peaks due to the passage of both fluorophores (and 4 due to simultaneous detection of a background peak in channel 0 and a peak due to NN 382 in channel 1). This represents a detection efficiency of $< 2\%$, as 4316 molecules labeled by both fluorophores are expected.

Figure 4 shows the normalized auto- and cross-correlation functions of the photon streams from the two detection channels. For channel 0 (IRD 700), the autocorrelation function $g00$ contains a peak near the origin with an amplitude of only ~ 1.07. The width of this peak is considerably shorter than $\sqrt{2}\delta_t = 0.7$ ms, which is the expected width if photodegradation and diffusion are negligible.[3] For channel 1 (NN 382), the autocorreleration function $g11$ has the expected Gaussian shape and width and has an amplitude clearly above 1. The cross-correlation function $g01(\tau)$ is peaked at negative delays τ, i.e. the peak occurs at about $g10$(0.45 ms). This indicates that most photons from

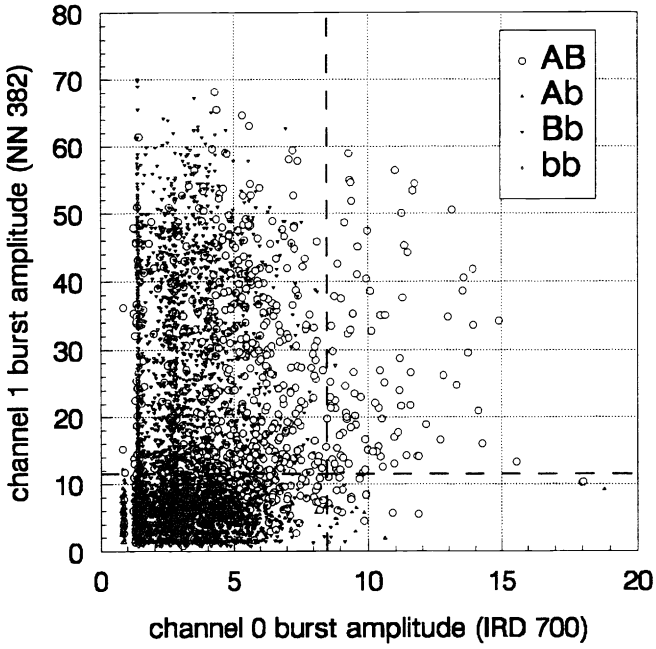

Figure 3. Plot of amplitudes of simultaneously detected bursts due to the following: AB: both fluorophores; Ab: IRD 700 in channel 0 and background in channel 1; Bb NN382 in channel 1 and background in channel 0; bb: background in both channels.

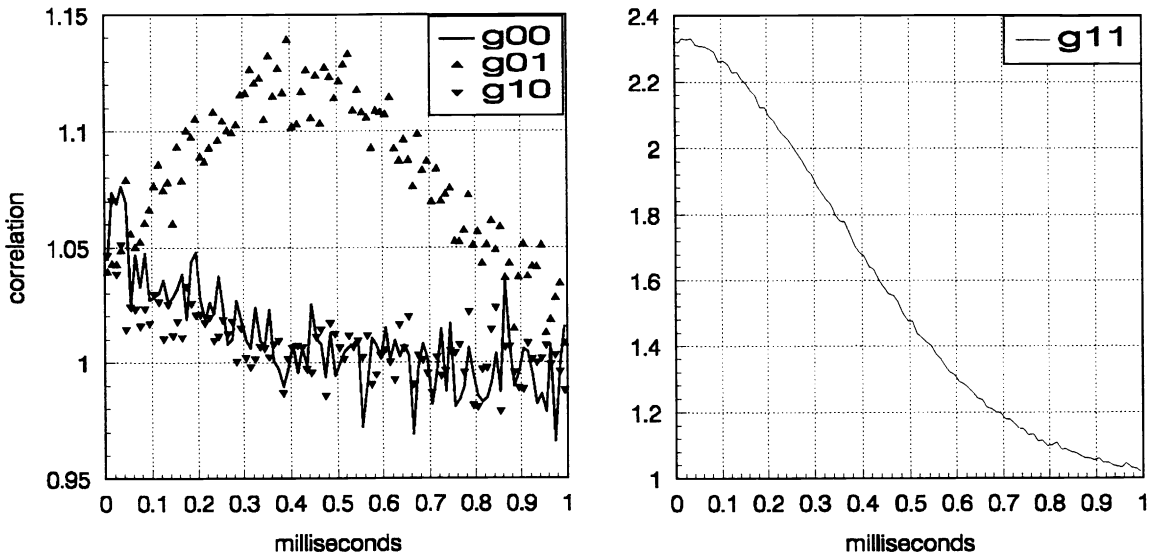

Figure 4. (a) Normalized autocorellation function of photon stream from channel 0 (g00); normalized cross-correlation functions between channels 0 and 1 (g01 and g10). (b) Normalized autocorellation function of photon stream from channel 1 (g11).

IRD 700 fluorophores occur when the molecule is ~ -0.45 ms $\times 6.9\mu$m/ms $= -3.1\mu$m from the center of the focused laser. Thus most IRD fluorophores are photodestroyed just as the molecule enters the laser beam.

The results in Figs. 2–4 have been obtained when 98% of the molecules contain both fluorophores. If only 1% of the molecules contain both fluorophores, but the total concentration of each fluorophore type remains the same, (i.e., total dye concentration 1.96×10^{-13}, fraction of each molecule type 0.01, 0.495, 0.495) then the histograms of burst amplitudes from each channel and the autocorrelation functions of each channel remain unchanged except for shot noise. However, for a simulation time of 100 s, the peak in the cross-correlatation function is lost, as it becomes smaller than the noise in the background, as shown in Fig. 5. Also, the number of simultaneously detected peaks does not provide a statistically significant measure of the presence of dual-labelled molecules. The mean number of such molecules expected to pass during the 100 s simulation time is 43.6. There are only 10 simultaneously detected peaks above the threshold levels of 8.5 and 11.5, of which 8 are caused by simultaneous detection of both fluorophores, as shown in Fig. 5b. If the simulation is re-run with the dual-labeled molecules replaced by equivalent concentrations of singly-labeled molecules, there are still 8 simultaneously detected peaks, 4 of which are caused by accidental simultaneous detection of both fluorophores. Nevertheless, in Pioneer's preliminary experiments with IRD 700 and NN 382, which used different operating conditions and data processing, simultaneous detection events were never seen.

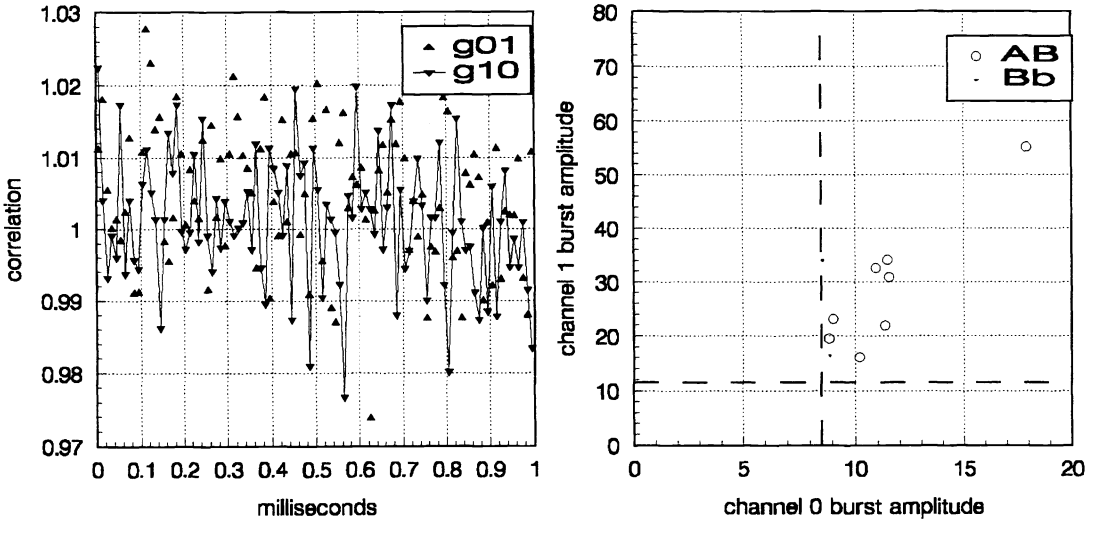

Figure 5. For a fraction of only 0.01 of the molecules containing both fluorophores: (a) Normalized cross-correlation functions between channels 0 and 1 (g01 and g10). (b) Plot of amplitudes of simultaneously detected bursts with values above 8.5 and 11.5.

For IRD 700 and NN 382, the simulation indicates that better performance should be possible by increasing the solution flow rate, so that IRD 700 fluorophores are less likely to become photodestroyed. Higher solution flow rates also enable a larger number of molecules to be sampled within the same measurement time. However, the photon bursts will be of lower amplitudes and the good detection efficiency for NN382 will be compromised. The real-time display of photon bursts becomes visually unappealing as it appears to differ little from that due just to shot noise fluctuations in the background, particularly for channel 0 (IRD 700). However, the shorter transit time enables use of a shorter integration time with the weighted sliding sum digital filter, so that the background becomes proportionately lower. Figure 6 shows that if all parameters are kept the same as those of Figs. 5a and b, but if the flow rate is increased by a factor of 10 and the widths of the Gaussian weights for the digital filter decreased by a factor of 10 to $\delta t = 50.7\mu$s, and 52.2μs, then a threshold setting of 2.5 results in the detection of 4550/43160 IRD 700 fluorophores with 1479 background events, and a threshold setting of 3.5 results in the detection of 15264/43160 NN 382 fluorophores with 1611 background events. Figure 7a shows that with these settings there are 351/436 simultaneous peaks due to both fluorophores, but a total of 646 false simultaneous detection events. However, if the thresholds are increased to 4.5 and 5.5, there are 25 simultaneous peaks due to both fluorophores

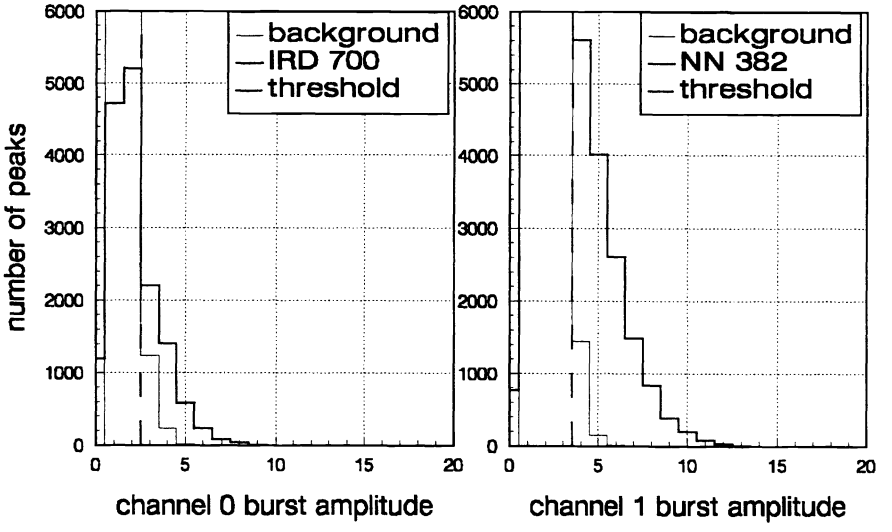

Figure 6. Flow velocity is increased ×10 compared to Fig. 5. Histograms of Gaussian weighted sliding sum peak amplitudes, due to background fluctuations and passage of (a) IRD 700, and (b) NN 382 fluorophores.

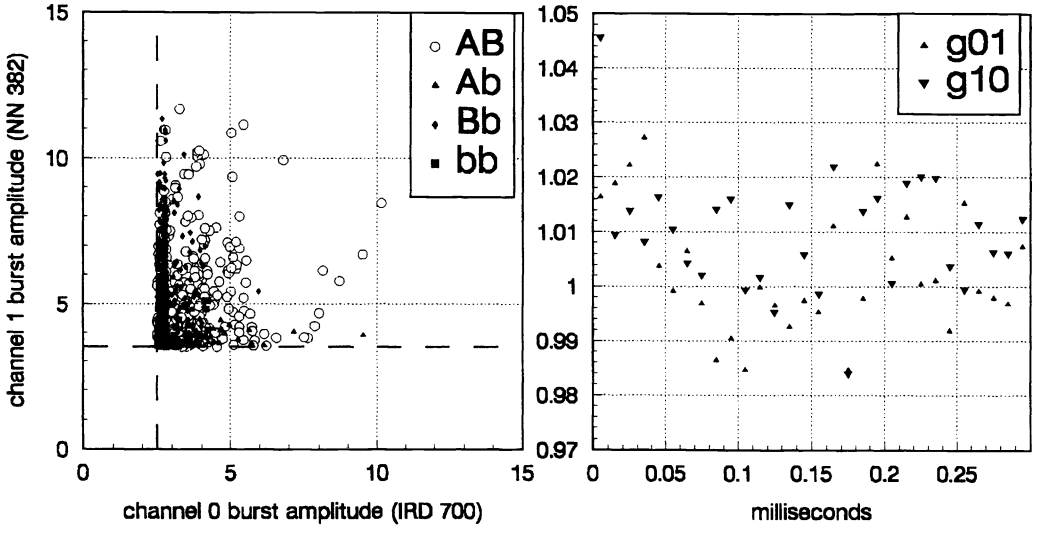

Figure 7. (a) Plot of amplitudes of simultaneously detected bursts, as in Fig. 5b, but with a ×10 increase in flow velocity. (b) Normalized cross-correlation function, as in Fig. 5a, but with a ×10 increase in flow velocity.

out of an expected 436 and 0 false detection events. If the dual-labeled molecules are then replaced by singly-labeled molecules, the number of simultaneously detected peaks is reduced to 15. Figure 7b presents the normalized cross-correlation function obtained under the fast-flow-rate conditions. The peak at the origin, which is expected to have a Gaussian shape with reduced width of $\sqrt{2}\delta_t = 0.07$ ms, is only barely seen, with $g10(0.005) = 1.045$. It is lost when dual-labeled molecules are removed from the simulation.

In the above results, the detection efficiency for IRD 700 is poor because of its low photostability. The following question of hence of interest: Would considerably better performance be achieved with the use of hybridization probes containing two rather than one IRD 700 fluorophore? The simulation indicates that if 1 % of the 1.96×10^{-13} M concentration of molecules are labeled by 2 rather than 1 IRD 700 fluorophores, and 1 NN 382 fluorophore, but if all

other parameters are the same as those in Figs. 5 and 7 respectively, then there is a noticeable increase in the number of simultaneously-detected photon bursts. For the 50 μl/min flow velocity, for threshold settings of 8.5 and 11.5, the number of such peaks is increased from 8 to 17 (with 43.6 expected) and there are 2 false detection events. With the dual-labeled molecules replaced by singly-labeled molecules, the number of simultaneously detected peaks is reduced to 8. However, the cross-correlation function still does not show a peak. For the 500 μl/min flow velocity, and with thresholds of 4.5 and 5.5, the number of simultaneous peaks is increased from 25 to 34 (with 436 expected) and there are again 0 false detection events. In this case, replacement of dual-labeled molecules results in 15 accidental simultaneous events. The cross-correlation function in this case shows a clearly-defined peak of amplitude $\sim$ 1.05, which is removed when the dual-labeled molecules are omitted from the simulation.

Another question of interest is the following: What performance could be expected if IRD 700 were to be replaced by a fluorophore with markedly better photostability, such as LJB? Graphs of results generated for LJB are not shown here due to space restrictions, but the conclusions are as follows: If the full 1 mW of laser excitation power is used in each laser beam, the flow rate is 50 μl/min, and threshold values of 11.5 are used at each detection channel, then the predicted detection efficiency for LJB is 110 %. The $>$ 100% detection efficiency arises because some of the fluorophores that pass through the periphery of the laser beam, beyond the $1/e^2$ intensity profile, are still sufficiently excited for detection. Another cause is that occasionally a background fluctuation near to a molecule photon burst will contain one or more fluorescence photons from the molecule, causing the simulation to identify the burst as being due to the molecule, and thereby double-counting the molecule. The false detection rate is 1.21 s^{-1}. For a simulated experiment time of 100 s, the auto- and cross-correlation functions exhibit clear peaks at the origin, even when the fraction of dual-labeled molecules is only 0.01 for a total fluorophore concentration of 1.96×10^{-13} M. The number of peaks that are simultaneously detected within $\pm 1.5 \times \delta_t$ is 182 due to both fluorophores and 23 due to false events. However, only 85 dual-labeled molecules are expected. Thus most simultaneous detection events are accidental coincidences, which have increased considerably in number because each channel now has efficient detection. Such accidental coincidences are not expected to contribute to the cross-correlation function, and indeed, if the dual-labeled molecules are removed from the simulation, the peak in the cross-correlation function vanishes, while 151 simultaneously occuring peaks remain.

If accidental coincidences are to be avoided in the data analysis, lower overall solution concentrations should be used. For the faster flow rate of 500 μl/min, a total concentration of only 1.96×10^{-14} M and 0.01 fraction of dual-labeled molecules, there are 25 simultaneous peaks above thresholds of 4.5, with 3 being due to background, for a simulation time of 100 s. When the dual-labeled molecules are replaced by singly-labeled ones, 7 simultaneous peaks still remain. If the total concentration is increased to 1.96×10^{-12} M while keeping the fraction of dual-labeled molecules at 0.01, there are so many accidental coincidences that the presence of dual-labeled molecules is not apparent from the number of simultaneous peaks. However, the cross-correlation function exhibits a clear peak after a simulation time of only 10 s. The peak is removed if the dual-labeled molecules are replaced by equivalent concentrations of singly-labeled molecules. Thus the cross-correlation function appears to be a more robust analysis method for rapid detection of dual-labeled molecules.

Finally, LJB has wonderful characteristics for SMD but unfortunately it is stereochemically difficult to attach to a DNA hybridization probe. If this problem can be overcome, then rapid gene detection with infrared diode lasers should be readily achievable using LJB together with NN 382.

REFERENCES

1. A. Castro, and J. G. K. Williams, "Single-molecule detection of specific nucleic acid sequences in unamplified genomic DNA," *Anal. Chem.* **69**, pp. 3915–3920, 1997.
2. S. A. Soper, E. B. Shera, L. M. Davis, H. L. Nutter, and R. A. Keller, "The photophysical constants of several fluorescent dyes pertaining to ultrasensitive fluorescence spectroscopy," *Photochem. and Photobiol.* **57**, pp. 972–977, 1993.
3. D. H. Bunfield, and L. M. Davis, "Monte Carlo simulation of a single-molecule detection experiment," *Appl. Opt.* **37**, pp. 2315–2326, 1998.
4. T. S. Lundgren, E. M. Sparrow, and T. B. Starr, *J. Basic Eng.*, **86**, pp. 620–626, 1964.
5. R. Loudon, *The Quantum Theory of Light*, 1st. ed., Clarendon Press, Oxford, 1973, p. 210.